

1 **Nonlinear discrete homogenized model for masonry walls out-of-plane loaded**

2

3 Luís C. Silva⁽¹⁾, Paulo B. Lourenço⁽²⁾, Gabriele Milani⁽³⁾

4

5 ¹ PhD candidate, Dept. of Civil Engineering, ISISE, University of Minho, Azurém,

6 4800-058 Guimarães, Portugal. E-mail: luisilva.civil@gmail.com

7 ² Full Professor, Dept. of Civil Engineering, ISISE, University of Minho, Azurém, 4800-

8 058 Guimarães, Portugal. E-mail: pbl@civil.uminho.pt

9 ³ Associate Professor, Department of Architecture, Built environment and Construction

10 engineering (A.B.C.), Technical University in Milan, Piazza Leonardo da Vinci 32,

11 20133 Milan, Italy. E-mail: gabriele.milani@polimi.it

12 Keywords: masonry, out-of-plane, homogenization, nonlinear, DEM

13 **Abstract**

14 A simple and reliable homogenization approach coupled with rigid elements and
15 homogenized interfaces for the analysis of out-of-plane loaded masonry panels is
16 presented.

17 The homogenization approach proposed is a coarse FE discretization where bricks are
18 meshed with a few elastic constant stress triangular elements and joints reduced to
19 interfaces with elasto-plastic softening behavior with friction, tension cutoff and a cap in
20 compression. Flexural behavior is deduced from membrane homogenized stress-strain
21 relationships through thickness integration (Kirchhoff-Love plate hypothesis). The
22 procedure is robust and allows obtaining homogenized bending moment/torque curvature
23 relationships (also in presence of membrane pre-compression) to be used at a structural
24 level within a Rigid Body and Spring Mass model (RBSM) implemented in the
25 commercial code ABAQUS. The model relies in rigid quadrilateral elements

26 interconnected by homogenized bending/torque nonlinear springs. The possibility of
27 extending the procedure to the FE-package ABAQUS, with standard built-in solution
28 procedures, allows for a robust reproduction of masonry out-of-plane behavior beyond
29 the peak load, in presence of global softening.

30 The procedure is tested on a set of windowed and full masonry panels in two-way
31 bending. Excellent agreement is found both with experimental data and previously
32 presented numerical approaches.

33 **Introduction**

34 Out-of-plane failure of masonry occurs at very low levels of the horizontal actions and
35 there are three main features to deal with in a numerical model devoted to the analysis of
36 masonry in bending: (1) the role of vertical membrane pre-compression, (2) masonry
37 orthotropic behavior due to the arrangement of the units, and (3) possible failure due to
38 out-of-plane shear in case of thick walls. A vertical membrane pre-compression, typically
39 due to masonry self-weight and gravity loads in general, plays a fundamental role in the
40 increase in the ductility and the out-of-plane strength, as extensively shown by Milani
41 and Tralli (2011).

42 Masonry orthotropy is evident for walls exhibiting a regular texture. Masonry units
43 staggering is responsible for a horizontal bending (i.e. with rotation along a vertical axis)
44 stiffer and more resistant than the vertical one (i.e. with rotation along a horizontal axis),
45 as the bed joint contributes in torque to increase stiffness and strength. Orthotropy tends
46 to become more evident with the progressive degradation of the material. The different
47 topology of the continuous horizontal joints with respect to the vertical ones, interrupted
48 by the blocks, implies that tangential stresses acting on bed joints tend to play a significant
49 role in the horizontal bending increase, while they are not relevant in vertical bending.
50 Micro-modelling, relying into the distinct discretization of units and mortar (usually

51 reduced to interface to speed up computations) is certainly capable of well reproducing
52 out-of-plane orthotropy, see for instance Macorini & Izzuddin (2011) and Macorini &
53 Izzuddin (2013), but such procedure is characterized by long processing times and a large
54 number of degrees of freedom, sometimes requiring parallelization.

55 Considering the difficulties, it can be affirmed that at present a macro-scale computational
56 approach is still needed. Macro-modelling (Dhanasekar et al. 1985; Lourenço 1997, 2000;
57 Pelà et al. 2013) allows studying large scale structures without the drawbacks exhibited
58 by micro-modelling, because the heterogeneous assemblage of mortar and bricks is
59 substituted at a structural scale with a fictitious homogeneous anisotropic material. The
60 calibration of the model is however cumbersome, as a consequence of the high level of
61 sophistication, usually needing several inelastic parameters to set, requiring expensive
62 experimental campaigns and data (Lourenço et al. 1998).

63 It is noted that it is not straightforward to account for tangential stresses acting along the
64 out-of-plane direction. This would require to deal with 3D models at the meso-scale, as
65 well as to adopt 3D strength domains and 3D inelastic strain evolution laws for mortar
66 joints reduced to interfaces. For running bond and generally for single or two-wythes
67 walls (e.g. English or Flemish bond) with slenderness greater than 8-10, it has been shown
68 by different authors (Casolo and Milani 2010; Cecchi et al. 2007; Cecchi and Milani 2008;
69 Milani et al. 2006) that the assumption of the thin plate Kirchhoff–Love hypothesis is
70 adequate and that out-of-plane sliding can occur on limited portions of the walls, mainly
71 near corners or under concentrated loads. Therefore, at the macro-scale, damage
72 mechanisms can be reasonably described assuming a thin plate hypothesis, i.e. where
73 inelastic dissipation is mainly due to the combination of vertical, horizontal bending and
74 torsion. Considering the aforementioned key issues characterizing masonry subjected to

75 out-of-plane loading, a simple two-step model is used here to analyze efficiently masonry
76 panels in bending.

77 In such a framework, homogenization (see e.g Luciano and Sacco 1997; de Buhan and de
78 Felice 1997; Mistler et al. 2007; Milani 2011) is probably the most efficient compromise
79 between micro- and macro-modelling, because it allows in principle to perform nonlinear
80 analyses of engineering interest without a distinct representation of bricks and mortar, but
81 still taking into account their mechanical properties and masonry texture at a cell level.

82 Homogenization (or related simplified approaches) is essentially an averaging procedure
83 performed at a meso-scale on a representative element of volume (RVE), which generates
84 the masonry pattern by repetition. On the RVE, a Boundary Value Problem BVP is
85 formulated, allowing an estimation of the expected average masonry behavior to be used
86 at structural level. The resultant material obtained is orthotropic, with softening in both
87 tension and compression. A straightforward approach to solve BVPs at the meso-scale is
88 based on Finite Elements (FEs) (Massart et al. 2007; Mercatoris and Massart 2011), where
89 bricks and mortar are either elasto-plastic with softening or damaging materials. It is also
90 known as a multilevel finite element method (FE²), which essentially is a twofold
91 discretization, the first for the unit cell and the second at structural level. However, FE²
92 appears still rather demanding, because a new BVP has to be solved numerically for each
93 load step, in each Gauss integration point.

94 In order to circumvent such a limitation, a two-step homogenization procedure is hereafter
95 proposed. In the first step, masonry is substituted with a macroscopic equivalent material
96 through a simplified homogenization model in which the unit cell is subdivided into
97 several layers along the thickness. The choice of concentrating non-linearity on the
98 interfaces appears particularly suitable because: (1) it allows limiting the computational
99 effort required to perform full scale analyses to a great extent, and; (2) it seems in

100 agreement with experimental evidence, clearly showing a damage propagation
101 zigzagging along joints. Considering a single masonry layer, the RVE is discretized
102 through triangular elastic plane stress elements (blocks) and nonlinear interfaces (mortar
103 joints). The procedure is robust and allows obtaining homogenized bending
104 moment/torque curvature relationships (also in presence of membrane pre-compression)
105 to be used at a structural level.

106 In the second step, entire masonry walls are analyzed in the nonlinear range by means of
107 a Rigid Body and Spring Mass model (RBSM) implemented in the commercial code
108 Abaqus (2006). The RBSM model relies into a discretization with rigid quadrilateral
109 elements interconnected by homogenized bending/torque nonlinear springs. It is stressed
110 that the RBSM model is not available in ABAQUS, but it can be easily implemented
111 utilizing the FEs gallery available in any commercial code. Standard arc-length routines
112 already built in Abaqus (2006) allow for a robust reproduction of out-of-plane masonry
113 behavior beyond the peak load, in presence of global softening. The latter addresses the
114 main drawback of previous work (Milani and Tralli 2011) whereby an energy-based
115 formulation at a structural scale was used, through a quadratic-programming approach,
116 which assumed linear piecewise discontinuous functions for the homogenized bending
117 curves to be able to account for material softening. The main novelty of the present study
118 is that it allows using homogenized curves, derived from the foregoing scale, without the
119 need of further simplifications to reproduce softening.

120 Two sets of structural comparisons are discussed here to show the capabilities of the
121 procedure proposed, the first on solid walls and the second on windowed panels in two-
122 way bending, for which global pressure-displacement and crack patterns are available
123 from both experimental data and previously presented numerical models.

124 **Out-of-plane homogenized model**

125 A multi-scale approach is presented for the out-of-plane study of running-bond masonry
126 panels, as schematically described in Fig. 1a. The figure briefly shows the proposed flow-
127 work and the two-step strategy that firstly relies in a homogenization procedure at a meso-
128 scale. This theory focuses on the periodicity feature of a given media and it is therefore a
129 proper strategy for masonry (Pegon and Anthoine 1997). Again, the concept is based on
130 the mechanical characterization of a representative volume element (hereafter, RVE) by
131 solving a boundary value problem. Then, the study of the structure is accomplished
132 through the assemblage of these RVE units. The strategy allows defining the mechanical
133 properties of each material at the unit cell only, and obtaining the damage stress and strain
134 response by introducing considerations at the component level.

135 Several studies showed the clear advantages of this process. It allows a good trade-off
136 between consumed time and results accuracy and enables the study of real scale buildings,
137 see Milani and Tralli (2011), Milani and Venturini (2011), Casolo and Milani (2013),
138 Akhaveissy and Milani (2013) and Milani et al. (2007). The present out-of-plane
139 homogenization model is based on the initial in-plane identification of an elementary cell.
140 The main features of the in-plane homogenized model will be explained in what follows,
141 for further information the reader is recommended to Milani and Tralli (2011).

142 The RVE Y (or elementary cell) contains all the information necessary for describing the
143 macroscopic behavior of an entire wall. In brief, homogenization consists in introducing
144 averaged quantities for macroscopic strain and stress tensors (\mathbf{E} and $\mathbf{\Sigma}$, respectively). This
145 is the main concept of the homogenization process and implies that the macroscopic
146 stress $\mathbf{\Sigma}$ and strain \mathbf{E} tensors are calculated as given by Eq. (1):

$$147 \quad \mathbf{E} = \langle \boldsymbol{\varepsilon} \rangle = \frac{1}{V} \int_Y \boldsymbol{\varepsilon}(\mathbf{u}) dY ; \quad \mathbf{\Sigma} = \langle \boldsymbol{\sigma} \rangle = \frac{1}{V} \int_Y \boldsymbol{\sigma} dY \quad (1)$$

148 where $\langle * \rangle$ is the average operator, $\boldsymbol{\varepsilon}$ is the local strain value, which is directly dependent
 149 on the displacements field \mathbf{u} , $\boldsymbol{\sigma}$ is the local stress value and V is the volume of the
 150 elementary cell.

151 The homogenization procedure allows to describe the macroscopic level through the
 152 meso-scale by means of an upward scheme. All the mechanical quantities are considered
 153 as additive functions and periodicity conditions are imposed on the stress field $\boldsymbol{\sigma}$ (see
 154 Eq.(2) and the displacement field u (see Eq.(3)) (Anthoine 1995), so that:

$$155 \quad \boldsymbol{\sigma} \text{ periodic on } \partial Y \text{ and } \boldsymbol{\sigma} \mathbf{n} \text{ antiperiodic on } \partial Y_1 \quad (2)$$

$$156 \quad \mathbf{u} = \mathbf{E} \mathbf{y} + \mathbf{u}^{per} \text{ periodic on } \partial Y_1 \quad (3)$$

157 where \mathbf{u}^{per} stands for a periodic displacement field. It may be noted that the periodic
 158 displacement fluctuation \mathbf{u}^{per} in Eq.(3) enforces the boundary segments of the RVE to
 159 have the same deformed configuration, see Fig. 1b.

160 In the present model, the RVE is constituted by joints reduced to interfaces with zero
 161 thickness and elastic bricks. Bricks are discretized by means of a coarse mesh constituted
 162 by plane-stress triangles, Fig. 1b. Likewise, brick-brick interfaces are elastic and therefore
 163 they do not contribute on the inelastic deformation of the unit cell. The utilization of
 164 brick-brick interfaces may be useful when dealing with low strength units. Here, it is
 165 assumed that all the nonlinearity in the RVE is concentrated exclusively on joint
 166 interfaces. The elastic domain of joints is bounded by a composite yield surface that
 167 includes tension, shear and compression failure with softening. A multi-surface plasticity
 168 model is adopted, with softening, both in tension and compression (see Fig. 1b). The
 169 joints failure is ruled by a classical Mohr-Coulomb type strength criterion, with a tension
 170 cut-off and a linear compression cap. The parameters f_t and f_c are, respectively, the tensile
 171 and compressive strength of the mortar, c is the cohesion, Φ is the friction angle, and Ψ
 172 is the angle which defines the linear compression cap. For the tension mode, exponential

173 softening on the tensile strength is assumed with an associated flow-rule. The yield
 174 function reads:

$$175 \quad f_1(\boldsymbol{\sigma}, \kappa_1) = \boldsymbol{\sigma} - f_0 e^{\frac{f_{t0}}{G_f} \kappa_1} \quad (4)$$

176 where f_{t0} is the initial joint tensile strength, G_f^I is the mode-I fracture energy and κ_1 is a
 177 scalar that controls the amount of softening. For the shear mode, a Mohr-Coulomb yield
 178 function with a non-associated flow rule is considered:

$$179 \quad f_2(\boldsymbol{\sigma}, \kappa_2) = |\tau| + \boldsymbol{\sigma} \times \left(\tan(\phi_0) + \frac{(\tan(\phi_t) - \tan(\phi_0))(c_0 - c)}{c_0} \right) - c_0 e^{\frac{c_0}{G_f^{II}} \kappa_2} \quad (5)$$

180 where c_0 is the initial cohesion, $\tan(\phi_0)$ the initial friction angle, $\tan(\phi_t)$ the residual
 181 friction angle and G_f^{II} is the mode-II fracture energy. For the compression mode, an
 182 associated elastic-perfectly plastic behavior is assumed, with a yield function described
 183 as follows:

$$184 \quad f_3(\boldsymbol{\sigma}) = |\tau| + (\boldsymbol{\sigma} + f_c) \tan(\Psi) \quad (6)$$

185 where f_c is the uniaxial compressive strength and Ψ is the angle that defined the linear
 186 compression cap. The properties adopted for the present study are gathered on Table 1.
 187 The latter information is related with the experimental data used for the validation step at
 188 a structural level of the proposed discrete model.

189 The response of the RVE under out-of-plane actions is obtained subdividing the thickness
 190 into several n layers (40 layers are assumed). A displacement driven approach is adopted,
 191 meaning that macroscopic curvature increments $\Delta\chi_{11}$, $\Delta\chi_{22}$, $\Delta\chi_{12}$ are applied through
 192 suitable periodic boundary displacement increments. Thus, each layer undergoes only in-
 193 plane displacements and may be modelled through plane stress FEs. Each increment
 194 defines the number of discrete data points of σ - ε and M - θ curves.

195 Thus, a bending moment-curvature relationship is obtained for each interface angle;
 196 through the obtained RVE macroscopic mode-I stresses. The latter failure mode

197 assumption is valid once masonry presents in general low compressive stresses at failure.
 198 Being a low-tensile strength material, the cross-section failure is ruled by tensile cracking
 199 and a linearized behavior in compression is considered, with stiffness degradation present
 200 only in tension. Towards the derivation of the M - θ curve for each interface, the cross-
 201 section equilibrium is iteratively calculated accounting for potential pre-compression
 202 states. The bending moment capacity M of the cross section is calculated by the
 203 summation of each n_i layer contribution by means of the following equation:

$$204 \quad M = \sum_{i=1}^n \sigma_i \bar{d}_L dA_i \quad (7)$$

205 where σ_i is the mean stress at each layer, \bar{d}_L is the distance between the centroid of each
 206 layer and the neutral axis and dA_i is the area of each layer. The resultant moment M can
 207 also be simply written as the integral of stress multiplied by its distance from the middle
 208 section through the wall thickness:

$$209 \quad M = \langle \sigma y_3 \rangle = \frac{1}{A} \int_Y \sigma y_3 dY \quad (8)$$

210 In this way, homogenized curves are approximated to define the nonlinear flexural
 211 behavior of the interfaces. The on-thickness integration hypothesis allows evaluating
 212 moment-curvature diagrams for solid brick masonries, but can be easily adapted to hollow
 213 bricks assuming different mechanical properties for, e.g. internal and external layers. The
 214 latter procedure is represented in Fig. 2 for a horizontal interface, hereafter labelled with
 215 orientation $\theta = 90$ degrees, i.e. vertical bending. A similar strategy is performed to derive
 216 the torsion moment curve. Interface orientations are guided by the mesh representation of
 217 the discrete model at a structural scale. So, the implementation in a finite element package
 218 at a macro-scale allows to represent and study three-dimensional structures under out-of-
 219 plane actions.

220 **Structural discrete model**

221 On a macro-scale level, the out-of-plane analysis of the masonry walls is performed
222 through a novel discrete element mechanical system. The latter has support and
223 background in the works by Kawai (1977) and employs the information of the
224 homogenized curves at a structural scale. Simply, the discrete model is described as the
225 assemblage of quadrilateral rigid plates inter-connected on interface vertices by a set of
226 rigid beams and deformable trusses. The system of deformable trusses carries the material
227 information required for interfaces. A decoupled characterization of flexural and torsional
228 actions is adopted. In the mid-span of each interface a spherical hinge is positioned. The
229 aim is to allow the rotation for torsional movements as well as to guarantee the deformed
230 shape compatibility between adjoining elements. For a clear understanding of the model,
231 the discrete system is represented in Fig. 3.

232 Such discrete element approach is implemented into a commercial finite element
233 software, namely Abaqus (2006). The inherent advantages are mainly two. Firstly, the
234 robustness of the software to solve nonlinear static problems in presence of material
235 softening is obtained by means of an established arc-length procedure (Memon and Su
236 2004). Secondly, this allow a great potential to extend the model to structural applications
237 in any finite element software and the possibility to be used by professionals and
238 researchers.

239 **Material Properties: from meso- to macro-scale**

240 The masonry behavior when out-of-plane loaded is highly dependent on its anisotropy at
241 failure (Gilbert et al. 2006; Milani and Lourenço 2010). Experimental information
242 conducted on masonry walls in two-way bending shows that failure occurs for a relatively
243 ductile behavior and forming a well-defined path, see Chong et al. (1994) and
244 Southcombe et al. (1995).

245 Aiming at developing the required material information at a macro-scale, an identification
 246 of the desired mesh dimensions and geometrical characteristics of the walls may be
 247 performed. Bearing in mind that quadrilateral elements are assumed, two different angles
 248 are considered for the interfaces: 0 and 90 degrees. The behavior of the interfaces is
 249 obviously orthotropic with softening, because it derives from the aforementioned
 250 homogenization strategy. In this way, the homogenized bending moment-curvature and
 251 torsional moment-curvature curves of the interfaces is depicted in Fig. 4.

252 The procedure described in what follows is required to convert the latter information in
 253 valid input data for the FE package used at a structural scale. To accomplish this goal,
 254 obtaining stress and strain curves for each angle of the interface and for each bending
 255 moment direction is mandatory. Thus, the approach offers the possibility to reproduce the
 256 material orthotropy by defining different input stress-strain relationships according to the
 257 trusses' plane. The conversion between bending and torsion moment and stress values is
 258 achieved by Eq.(9) and (10):

$$259 \quad \sigma_{Axial\ truss} = \frac{M l_{influence}}{A_{Axial} t} \quad (9)$$

$$260 \quad \sigma_{Torque\ truss} = \frac{M l_{influence}}{A_{Torque} H} \quad (10)$$

261 Here, M is the bending moment, $l_{influence}$ is the influence length of each truss, t is the
 262 thickness of the wall, H the length of each quadrilateral panel, A_{Axial} is the axial truss area
 263 given by $0.25 \times t \times H$ and A_{Torque} is the torque truss area given by $0.5 \times e \times H$, where e (value
 264 of 10 mm) is the gap between the rigid plates, which ideally should be zero but in practice
 265 is assumed small enough to be able to place trusses between elements.

266 At last, the stress homogenized input curves may be properly calibrated. An elastic
 267 calibration for the stress curves is conducted. Briefly, by assuring the energy equivalence
 268 between the discrete mechanism and a homogeneous (for the masonry data, see Table 1)
 269 continuous shell element. The latter is guaranteed separately for both flexural and

270 torsional movements and so, a decoupled behavior is derived. For the sake of conciseness,
 271 the theoretical demonstration is not shown, but it can be easily derived that the Young's
 272 moduli of axial ($E_{flexural}$) and torque trusses (E_{torque}) are:

$$273 \quad E_{flexural} = \frac{E_{masonry}e}{12l_{influence}+6e} \frac{E_{masonry}}{(1-\nu^2)} \text{ and } E_{torque} = \frac{t^4}{3(2l_{influence}+e)H^2e} \frac{E_{masonry}}{(1+\nu)} \quad (11)$$

274 It is important to state that the present study focuses on the nonlinear static analysis of
 275 two sets of masonry panels. The walls under study were already experimentally out-of-
 276 plane tested at the University of McMaster and Plymouth by Gazzola and Drysdale (1986)
 277 and Chong et al. (1994), respectively. Also, it is highlighted that a refined mesh was
 278 defined for both case studies. The size of the interfaces (H), i.e. the side length of each
 279 quadrilateral panel, is only 100 mm.

280 In the first step, the holonomic homogenization model allows obtaining the macroscopic
 281 masonry material properties accounting for the strain softening regime. In the second step,
 282 this information should serve as input for the analysis at a structural level. Thus, the novel
 283 discrete element model implemented in the finite element package ABAQUS must be
 284 able to receive such data. The concrete damage plasticity model is selected for this
 285 purpose, as it allows to fully represent the inelastic behavior of masonry, by defining
 286 stress-strain curves for axial and torque trusses of the system. For further details
 287 concerning the model and its implementation, see Wahalathantri et al. (2011).

288 Simplified softening curves are considered for each truss, see for instance Fig. 5. To avoid
 289 convergence and run time problems, a small plateau near the peak of the curves is adopted
 290 in order to avoid abrupt stiffness losses. For the simulations, the post-failure stress-strain
 291 behavior must be introduced in the material information parameters. Specifically,
 292 ABAQUS requires the introduction of the cracking strain $\tilde{\epsilon}_t^{ck}$, which can be obtained for
 293 each point of the homogenized curve by Eq.(12):

$$294 \quad \tilde{\epsilon}_t^{ck} = \epsilon_t - \epsilon_0^{el} \quad (12)$$

295 where ε_o^{el} is the elastic strain corresponding to the undamaged material and ε_t is the total
296 strain of the holonomic curve. Damage parameters d_t should also be introduced, which
297 link the undamaged elastic modulus with that of the damaged material in the unloading
298 phase, as $E_d = E(1 - d_t)$, see also Fig. 5.

299 **Macro-scale validation: out-of-plane loaded masonry panels**

300 The macro-scale validation of the homogenization model is achieved by analyzing
301 masonry panels subjected to out-of-plane loads. The aim is to conclude about the ability
302 of the model to reproduce the nonlinear out-of-plane response of masonry. Available
303 experimental data of windowed and full panels in two-way bending are used. The panels
304 result from the studies of Gazzola and Drysdale (1986) at the University of McMaster
305 and Chong et al. (1994) at the University of Plymouth.

306 The first set of panels that are being studied refers to three running bond masonry panels
307 tested at the University of McMaster (Gazzola and Drysdale 1986). The panels are
308 designated as WII, WF and WPI. The geometry of the panels is similar, being the
309 boundary conditions the main difference, see Fig. 6. Such analyses allow to conclude
310 about the ability of the model to describe the response in terms of pressure vs. out-of-
311 plane displacements, and if the homogenized model is able to reproduce a pre-
312 compression state (due to the analysis in WPI panel).

313 Information concerning the assumed mechanical properties is reported in Table 1. The
314 out-of-plane behavior of a masonry wall is essentially ruled by the flexural strengths along
315 vertical and horizontal directions, which are available for both studied panels. The
316 properties identification is achieved by fitting the flexural strengths values with the ones
317 reported by Lourenço (1997). The same values for the horizontal flexural strength, $f_{tx} =$
318 0.81 (N/mm²), and for the vertical flexural strength, $f_{ty}=0.40$ (N/mm²), are adopted. The
319 bricks dimensions are $390 \times 190 \times 150$ mm³ and the thickness of the joints is 10 mm. The

320 same strategy is conducted for the Plymouth panels. Assuming bricks elastic and that the
321 non-linearity is restricted to the tensile regime, only mortar tensile strength and cohesion
322 can be tuned, with a fixed softening with pre-assigned fracture energy. It is believed that
323 the model is able to reproduce and predict well the response of masonry in the cases where
324 sufficient experimental information on its constituents is available.

325 The refined mesh with 100 mm of size has 1196 discrete elements for each panel (each
326 discrete element has 4 quadrilateral rigid plates). Whilst only collapse loads are reported
327 in Gazzola and Drysdale (1986), the results discussion addresses also the obtained
328 capacity curves. For each studied panel, Fig. 7 illustrates a comparison on global force-
329 displacement curves between the present model and: (i) the experimental collapse load
330 (McMaster university data), (ii) an anisotropic macro-model by Lourenço (2000) and (iii)
331 an upper and lower bond limit analysis by Milani et al. (2006).

332 For all the panels and regarding the collapse load, the present model allows to reach an
333 acceptable maximum error of 11% on peak experimental loads. Moreover, the pushover
334 curves present a similar shape when compared with those provided by the macro-model
335 proposed by Lourenço (2000). As aforementioned, the conducted analyses include a pre-
336 compression state only for the panel WPI. The homogenized model was prepared also to
337 compute the final stress-strain curves bearing a defined pre-compression state, assuming
338 that it is maintained constant during the out-of-plane loading.

339 The second set of out-of-plane experimental data is constituted by the panels tested at the
340 University of Plymouth by Chong et al. (1994). Five panels in running bond masonry
341 texture using solid clay bricks were tested and designated by SB (Chong et al. 1994;
342 Southcombe et al. 1995). The panels SB01 and SB05 have the same geometry, thus only
343 four panels (SB01-SB04) are considered and represented in Fig. 8. The boundary
344 conditions are the same for the four panels, i.e. laterally simply supported and fixed at the

345 base. The experimental investigation aimed at a better insight on the role played by the
346 openings size and shape.

347 The panels were loaded by air-bags until failure, whereas both the pressure and
348 displacement at the middle span of the free edge were monitored. Thus, the comparison
349 is here done in terms of pressure load and displacement in each masonry panel.

350 At a meso-scale, the mechanical properties adopted for the RVE characterization were
351 already presented in Table 1. Bearing that according to the experimental data (Chong et
352 al. 1994; Southcombe et al. 1995), the flexural uniaxial strengths f_{tx} and f_{ty} are 2.28 and
353 0.97 N/mm^2 , respectively, the mechanical properties adopted were tuned in order to fit
354 the latter values. The bricks dimensions are $215 \times 65 \times 102.5 \text{ mm}^3$ and the thickness of the
355 joints is 10 mm.

356 The refined mesh with 100 mm of size has 1122 discrete elements for panel SB01/05,
357 892 elements for panel SB02, 987 elements for panel SB03 and 960 elements for panel
358 SB04. It is important to stress that the mesh at the macro-scale is independent from the
359 mesh adopted in the RVE at a meso-scale and from the masonry texture, i.e. units'
360 geometry. Each nonlinear analysis, with the present refined mesh, took around 9 minutes
361 in a computer with an Intel Core i7-4710MQ 2.50 GHz processor. This running time
362 accounts for the pre-homogenization and calibration steps required before the analysis
363 and could be minimized, if (1) a coarser mesh is adopted or (2) by analyzing a half part
364 of the wall due to symmetry conditions. It is also important to understand that softening
365 is being represented and the associated convergence problems cannot be avoided.

366 Fig. 9 shows the comparison between the numerical and experimental results (Chong et
367 al. 1994), concerning pressure load and displacement at the middle node of the free edge.

368 In addition to the present model, other results are represented, namely an anisotropic
369 macro-model (Lourenço 2000), an elastic perfectly-plastic homogenized model

370 designated as EPP-model (Milani and Tralli 2011), a simplified deteriorating model based
371 on homogenized limit analysis designated as SD model (Milani and Tralli 2011) and
372 finally a simplified quadratic programming elastic-plastic model by Milani and Tralli
373 (2011), in which deterioration of interfaces (ultimate bending moment) is considered. For
374 the sake of conciseness, the reader is referred to Lourenço (2000) and Milani and Tralli
375 (2011), in order to analyze with further detail each of the aforementioned models.

376 In general, the comparison allows concluding that the obtained results are good, both in
377 terms of collapse load and displacements prediction, see Fig. 9. For the panel SB01/05
378 the failure pattern indicates that cracking occurs as expected due to flexural failure at the
379 fixed base of the wall, see Fig. 10. The cracking formation near the lateral supports, i.e.
380 diagonal cracks, is also clear. For further comparison with the experimental failure modes,
381 see Lourenço (1997). The peak load results are similar to the ones obtained
382 experimentally, even if the softening range starts slightly before than the other reference
383 curves.

384 For the second panel, designated as SB-02, the initial stiffness is marginally
385 overestimated. This panel is the one with the largest opening in height. Nevertheless,
386 reasonable agreement is found regarding the obtained peak load with a relative error of
387 around 20% with the experimental curve. The damage patterns show cracking due to
388 horizontal bending in the fixed base, vertical bending above the opening and the
389 formation of diagonal cracks surrounding the corners and lateral supports.

390 To what concerns panel SB03, both peak load and curve shape are quite similar to the
391 results by Lourenço (1997). The post-peak behavior is again characterized by the
392 formation of the vertical crack above the opening. Also, as expected, the formation of
393 diagonal cracks is evident at the opening sides and with the direction of the lateral
394 supports.

395 At last, the present model leads to a capacity curve with a reasonable agreement for the
396 panel SB04, in which the peak load has a relative error of around 10% with the macro-
397 model by Lourenço (1997). Similarly, a vertical crack above the opening is developed.
398 Failure due to torsional movements is also visible around the lateral supports, as well as
399 failure due to flexion at the base fixed support. The model is not able to directly follow
400 diagonal yield lines (zig-zag instead). Even so, the used quadrilateral mesh is refined
401 enough to minimize the mesh dependence and the differences concerning the
402 experimental results are not significant.

403 The results show the capacity of the model to obtain good representations of the nonlinear
404 behavior in panels with complex geometries, using refined meshes. The analyses of the
405 Plymouth panels are repeated with less refined meshes, see Fig. 11. The goal is to evaluate
406 the mesh dependence both in terms of results accuracy and running time duration. For the
407 first panel (SB-01/05) three medium-high refinement meshes (in respect with the brick
408 size) with edge size equal to 100, 150 and 200 mm, and two very coarse meshes, with
409 edge size equal to 500 and 1000 mm, are compared. Fig. 11a demonstrates that the mesh
410 dependency is low as the obtained difference on the pressure-displacement curve among
411 the meshes is less than 15%, for such large variation of mesh sizes, which is acceptable
412 from an engineering standpoint. In addition, it is worth noting that the required
413 computational time is impressively reduced for the coarse meshes (less than one minute),
414 but still reasonable for a strong mesh refinement, Fig. 11a (exponential reduction with the
415 increase of mesh size). The deformed shapes of panel SB-01/05 for the four refinement
416 levels studied are also presented in Fig. 11b.

417 On the other hand, only two refined meshes ($150 \times 150 \text{ mm}^2$ and $200 \times 200 \text{ mm}^2$) were
418 considered for the SB-02-04 panels to avoid geometrical misrepresentations, due to the
419 existence of openings. Regarding the running time duration, the coarser mesh (200×200

420 mm²) allows to obtain analyses times within 3 minutes only. For the peak load, the
421 differences between the studied meshes are lower than 5%, being therefore not relevant
422 for engineering applications. Some difference may be noted in the post-peak behavior,
423 but it is well known that rigid elements, where nonlinearity is concentrated on interfaces,
424 intrinsically suffer from limited mesh dependence on softening.

425 **Conclusions**

426 A two-step procedure was presented to study the nonlinear static behavior of masonry
427 panels subjected to out-of-plane loading, and allowing the use of any standard advanced
428 nonlinear finite element code. The first step concerns the homogenization model based
429 on an elastoplastic approach. This is performed at a meso-scale through a FE
430 discretization of the unit cell, the so-called representative volume element (RVE) and
431 allows obtaining the curvature-bending moment diagrams for each direction, i.e. masonry
432 orthotropy. For each layer, a plane-stress boundary problem was solved in which the
433 nonlinearity is concentrated only on joint interfaces, accounting for both tensile and
434 compressive strength and strain softening.

435 Being a new methodology, at a structural scale, the simulations were done within a novel
436 discrete element model implemented in the Finite Element software package Abaqus
437 (2006). The latter is composed by quadrilateral rigid plates connected by a system of rigid
438 beams, axial and torque trusses. This system represents the behavior of the homogenized
439 interfaces obtained previously. The obtained homogenized curves were calibrated and
440 then scaled in order to be readable by the software.

441 The validation of the model was performed through nonlinear static analyses on masonry
442 panels. The obtained peak loads have a good agreement with the experimental values with
443 an error less than 20% for the peak load. Also, the shape of the capacity curves was
444 compared with an anisotropic model. Good agreement was obtained between the capacity

445 curves and damage patterns between the complex anisotropic model and the new discrete
446 model, whereas a maximum peak load error of about 10% may be observed for the panel
447 SB-02. In addition, a mesh dependency test was conducted to deepen the knowledge on
448 refinement issues. One may note the importance of addressing the two following
449 recommendations to practitioners interested in a fast and reliable analysis of masonry
450 panels out-of-plane loaded: (i) the proposed homogenization-discrete element model does
451 not show critical mesh dependence issues. Very coarse meshes proved to predict well the
452 initial stiffness, ultimate load carrying capacity and ultimate ductility. The advantage of
453 the utilization of coarse meshes is certainly the considerable reduced computation effort
454 needed, see Fig. 11a. The only constraint is obviously in the correct definition of the
455 possible location of yield lines compatible with the real ultimate behavior of the walls.
456 On the other hand, (ii) as far as the previous precautions on the mesh generation are kept,
457 the only limitation in the utilization of few rigid elements is the impossibility to obtain a
458 detailed description of the actual crack patterns, to be compared with either experimental
459 ones or those obtained from expensive micro-modelling strategies. When such output is
460 needed, the user is recommended to refine the discretization.

461 At last, it is important to note the advantage of the procedure and its efficiency in respect
462 with a detailed heterogeneous micro-modelling strategy (i.e. a separate discretization of
463 bricks and mortar). The use of rigid plates minimizes the complexity regarding inelastic
464 phenomena problems. Using standard commercial FE packages, the effectiveness and
465 robustness of the software to solve problems accounting for the post-elastic behavior with
466 softening can be used. This also allows the possibility to extend the use of the proposed
467 model at professional level to fields such as earthquake or blast engineering. Regarding
468 the former, the use of truss beam elements that reproduces the homogenized behavior of
469 interfaces within a Concrete Damage Plasticity model at a macro-scale allows, in

470 principle, to conduct numerical analyses in the non-linear dynamic range. In addition, the
471 utilization of a robust commercial code like ABAQUS allows running analyses in the
472 non-linear dynamic range without any special difficulty, because the ex-novo
473 implementation of global solvers is not needed and proper hysteresis models are
474 available. On the other hand, in what concerns the latter, the application of the model in
475 the field of blast and impact engineering deserves a separate discussion because, in such
476 case, mechanical properties of the constituent materials are rate-dependent. A practical
477 way of proceeding would be to define the material properties using dynamic increase
478 factors.

479 **Acknowledgements**

480 This work was supported by FCT (Portuguese Foundation for Science and Technology),
481 within ISISE, scholarship SFRH/BD/95086/2013. This work was also partly financed by
482 FEDER funds through the Competitiveness Operational Programme - COMPETE
483 and by national funds through FCT – Foundation for Science and Technology within the
484 scope of the project POCI-01-0145-FEDER-007633.

485 **References**

- 486 Abaqus. (2006). “Dassault Systèmes Simulia Corporation.” RI: Dassault Systèmes Simulia
487 Corporation, Providence.
- 488 Akhaveissy, A. H., and Milani, G. (2013). “A numerical model for the analysis of
489 masonry walls in-plane loaded and strengthened with steel bars.” *International*
490 *Journal of Mechanical Sciences*, Elsevier, 72, 13–27.
- 491 Anthoine, A. (1995). “Derivation of the in-plane elastic characteristics of masonry
492 through homogenization theory.” *International Journal of Solids and Structures*,
493 32(2), 137–163.
- 494 de Buhan, P., and de Felice, G. (1997). “A homogenization approach to the ultimate
495 strength of brick masonry.” *Journal of the Mechanics and Physics of Solids*, 45(7),
496 1085–1104.
- 497 Casolo, S., and Milani, G. (2010). “A simplified homogenization-discrete element model
498 for the non-linear static analysis of masonry walls out-of-plane loaded.” *Engineering*
499 *Structures*, 32(8), 2352–2366.
- 500 Casolo, S., and Milani, G. (2013). “Simplified out-of-plane modelling of three-leaf
501 masonry walls accounting for the material texture.” *Construction and Building*
502 *Materials*, 40, 330–351.
- 503 Cecchi, A., and Milani, G. (2008). “A kinematic FE limit analysis model for thick English
504 bond masonry walls.” *International Journal of Solids and Structures*, 45(5), 1302–
505 1331.
- 506 Cecchi, A., Milani, G., and Tralli, A. (2007). “A Reissner–Mindlin limit analysis model
507 for out-of-plane loaded running bond masonry walls.” *International Journal of*
508 *Solids and Structures*, 44(5), 1438–1460.
- 509 Chong, V., Southcombe, C., and May, I. (1994). “The behavior of laterally loaded

510 masonry panels with openings.” *Proceedings of 3rd international masonry*
511 *conference. London, UK: Proceedings of the British Masonry Society*, 178–82.

512 Dhanasekar, M., Kleeman, P., and Page, A. (1985). “The failure of brick masonry under
513 biaxial stresses.” *ICE Proceedings*, Thomas Telford, 79(2), 295–313.

514 Gazzola, E. A., and Drysdale, R. G. (1986). “A Component Failure Criterion for
515 Blockwork in Flexure.” *Advances in Analysis of Structural Masonry*, ASCE, 134–
516 154.

517 Gilbert, M., Casapulla, C., and Ahmed, H. M. (2006). “Limit analysis of masonry block
518 structures with non-associative frictional joints using linear programming.”
519 *Computers & Structures*, 84(13–14), 873–887.

520 Kawai, T. (1977). “New Discrete Structural Models and Generalization of the Method of
521 Limit Analysis.” *Finite Elements in Nonlinear Mechanics*, P.G. Bergan et al. eds,
522 Tapir Publishers, 885–906.

523 Lourenço, P. B. (1997). “An anisotropic macro-model for masonry plates and shells:
524 implementation and validation.” *TNO Building and Construction Research -*
525 *Computational Mechanics*, (report no. 03.21.1.31.07), 34–91.

526 Lourenço, P. B. (2000). “Anisotropic Softening Model for Masonry Plates and Shells.”
527 *Journal of Structural Engineering*, American Society of Civil Engineers, 126(9),
528 1008–1016.

529 Lourenço, P. B., Rots, J. G., and Blaauwendraad, J. (1998). “Continuum Model for
530 Masonry: Parameter Estimation and Validation.” *Journal of Structural Engineering*,
531 American Society of Civil Engineers, 124(6), 642–652.

532 Luciano, R., and Sacco, E. (1997). “Homogenization technique and damage model for
533 old masonry material.” *International Journal of Solids and Structures*, 34(24),
534 3191–3208.

535 Macorini, L., and Izzuddin, B. A. (2011). “A non-linear interface element for 3D
536 mesoscale analysis of brick-masonry structures.” *International Journal for*
537 *Numerical Methods in Engineering*, 85(12), 1584–1608.

538 Macorini, L., and Izzuddin, B. A. (2013). “Nonlinear analysis of masonry structures using
539 mesoscale partitioned modelling.” *Advances in Engineering Software*, 60–61, 58–
540 69.

541 Massart, T. J., Peerlings, R. H. J., and Geers, M. G. D. (2007). “An enhanced multi-scale
542 approach for masonry wall computations with localization of damage.” *International*
543 *Journal for Numerical Methods in Engineering*, John Wiley & Sons, Ltd., 69(5),
544 1022–1059.

545 Memon, B.-A., and Su, X. (2004). “Arc-length technique for nonlinear finite element
546 analysis.” *Journal of Zhejiang University. Science*, 5(5), 618–28.

547 Mercatoris, B. C. N., and Massart, T. J. (2011). “A coupled two-scale computational
548 scheme for the failure of periodic quasi-brittle thin planar shells and its application
549 to masonry.” *International Journal for Numerical Methods in Engineering*, John
550 Wiley & Sons, Ltd., 85(9), 1177–1206.

551 Milani, G. (2011). “Simple homogenization model for the non-linear analysis of in-plane
552 loaded masonry walls.” *Computers & Structures*, 89(17), 1586–1601.

553 Milani, G., and Lourenço, P. B. (2010). “A simplified homogenized limit analysis model
554 for randomly assembled blocks out-of-plane loaded.” *Computers & Structures*,
555 88(11–12), 690–717.

556 Milani, G., Lourenço, P., and Tralli, A. (2006). “Homogenization Approach for the Limit
557 Analysis of Out-of-Plane Loaded Masonry Walls.” *Journal of Structural*
558 *Engineering*, American Society of Civil Engineers, 132(10), 1650–1663.

559 Milani, G., Lourenço, P., and Tralli, A. (2007). “3D homogenized limit analysis of

560 masonry buildings under horizontal loads.” *Engineering Structures*, 29(11), 3134–
561 3148.

562 Milani, G., and Tralli, A. (2011). “Simple SQP approach for out-of-plane loaded
563 homogenized brickwork panels, accounting for softening.” *Computers & Structures*,
564 89(1–2), 201–215.

565 Milani, G., and Venturini, G. (2011). “Automatic fragility curve evaluation of masonry
566 churches accounting for partial collapses by means of 3D FE homogenized limit
567 analysis.” *Computers & Structures*, 89(17–18), 1628–1648.

568 Mistler, M., Anthoine, A., and Butenweg, C. (2007). “In-plane and out-of-plane
569 homogenisation of masonry.” *Computers & Structures*, 85(17), 1321–1330.

570 Pegon, P., and Anthoine, A. (1997). “Numerical strategies for solving continuum damage
571 problems with softening: Application to the homogenization of Masonry.”
572 *Computers & Structures*, 64(1–4), 623–642.

573 Pelà, L., Cervera, M., and Roca, P. (2013). “An orthotropic damage model for the analysis
574 of masonry structures.” *Construction and Building Materials*, 41, 957–967.

575 Southcombe, C., May, I., and Ching, V. (1995). “The behavior of brickwork panels with
576 openings under lateral load.” *Proceedings of the 4th international masonry
577 conference, vol. 1*, British Masonry Society, London, 105–10.

578 Wahalathantri, B. L., Thambiratnam, D., Chan, T., and Fawzia, S. (2011). “A material
579 model for flexural crack simulation in reinforced concrete elements using
580 ABAQUS.” *Proceedings of the First International Conference on Engineering,
581 Designing and Developing the Built Environment for Sustainable Wellbeing*,
582 Queensland University of Technology.

583

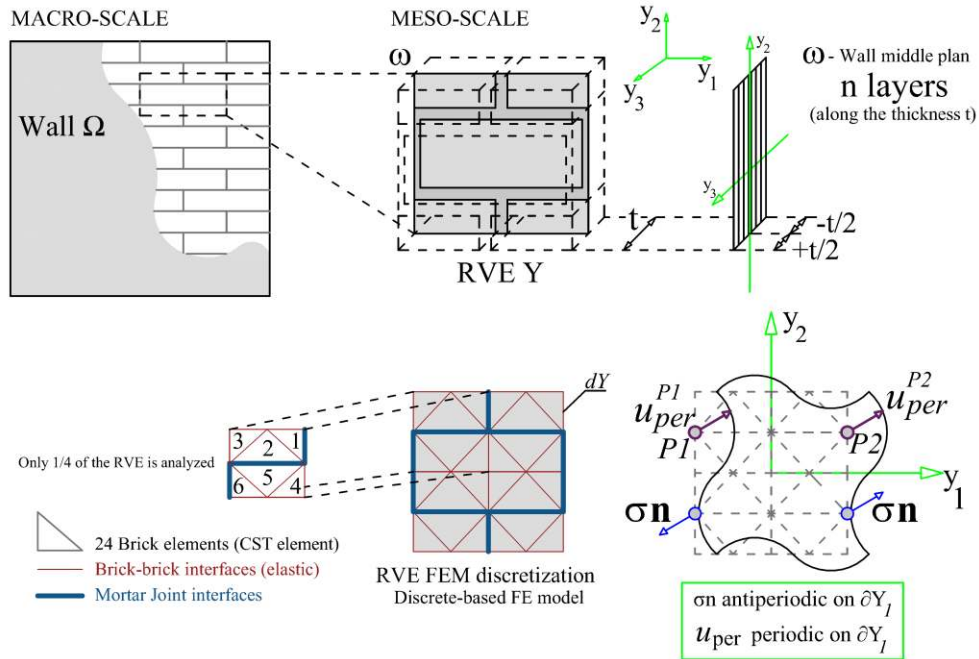
584

(a)

FLOW-CHART

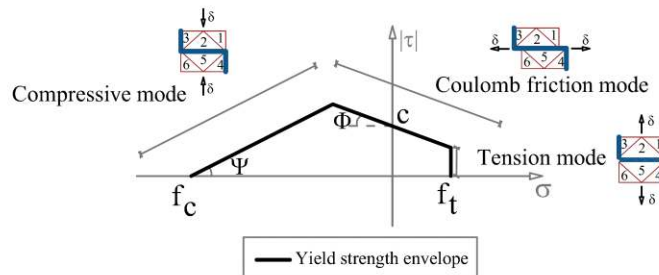


(b)



(c)

Modified Mohr-Coulomb for mortar joints

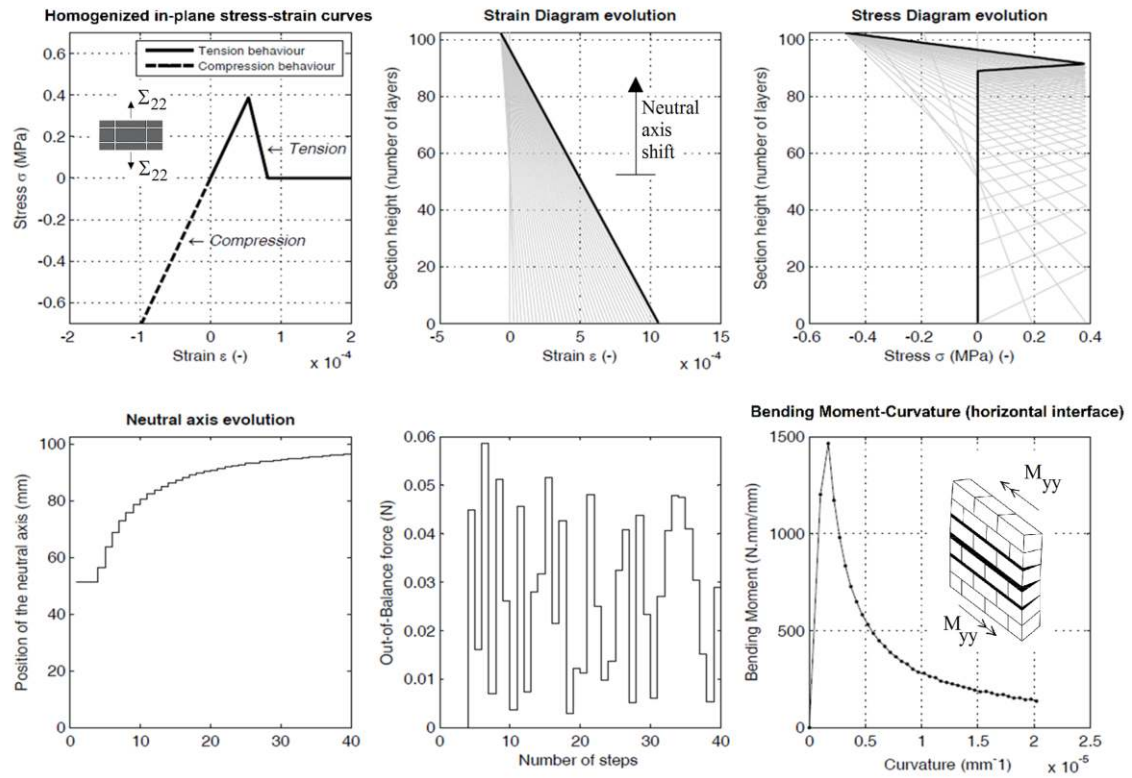


585

586 **Fig. 1.** (a) Flow-chart of the present two-step procedure; (b) Micro-mechanical model

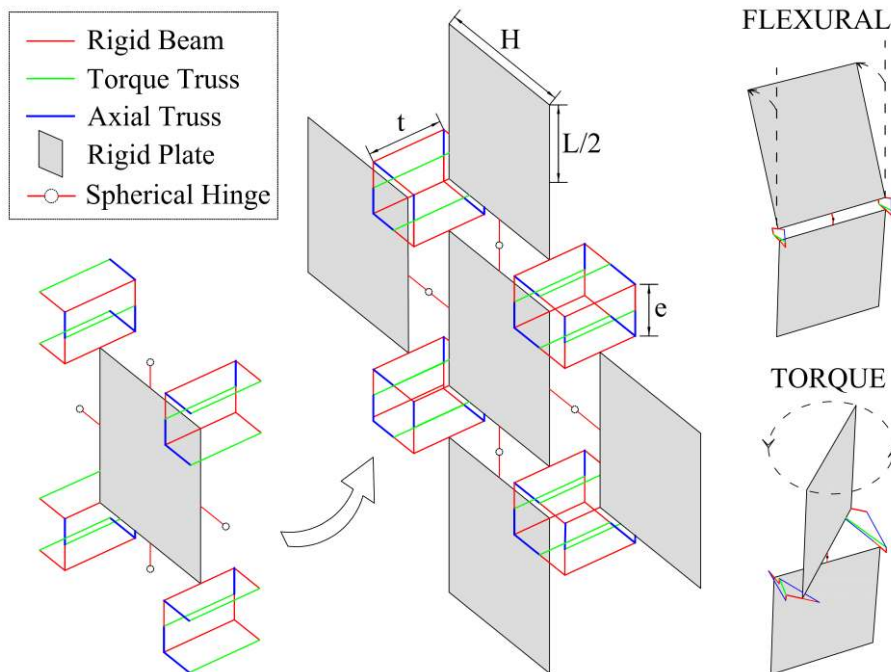
587 adopted for the present homogenized model; and (c) strength domain for joints reduced

588 to interfaces.



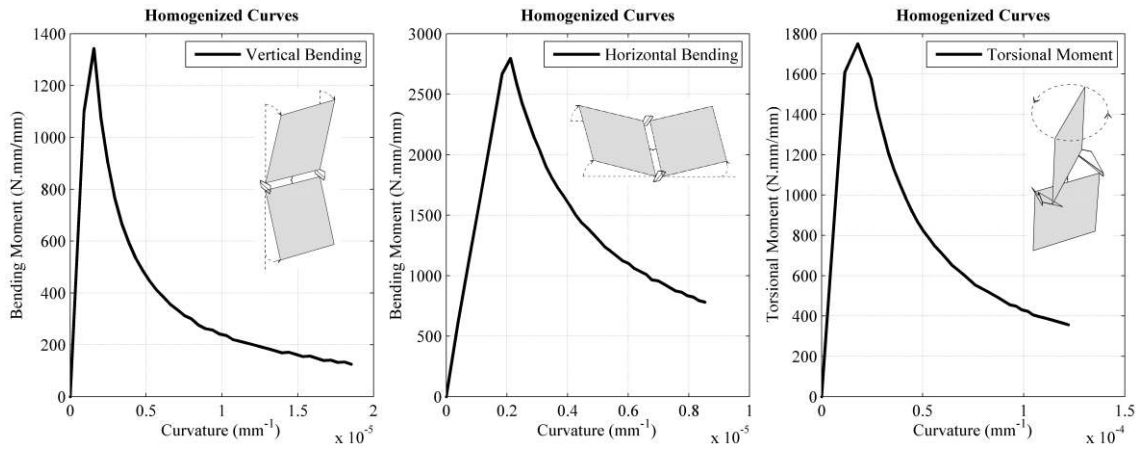
589

590 **Fig. 2.** Adopted procedure to derive out-of-plane homogenized bending moment-
 591 curvature curves (e.g. vertical bending).



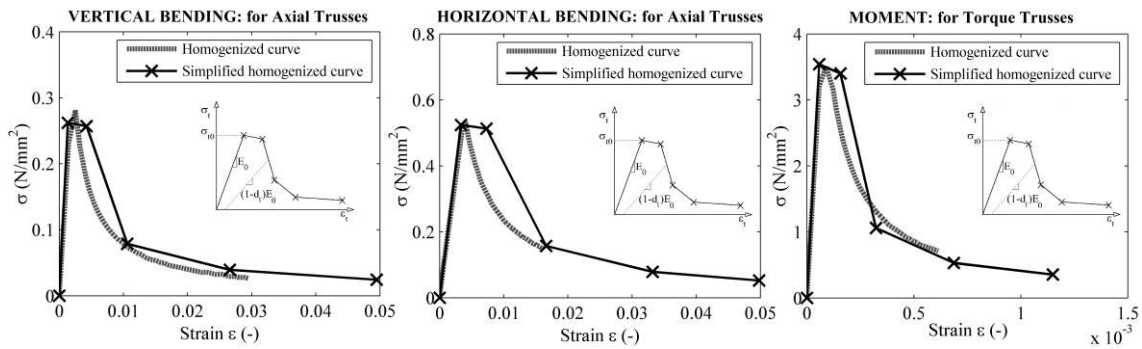
592

593 **Fig. 3.** Description of the novel discrete element system proposed.



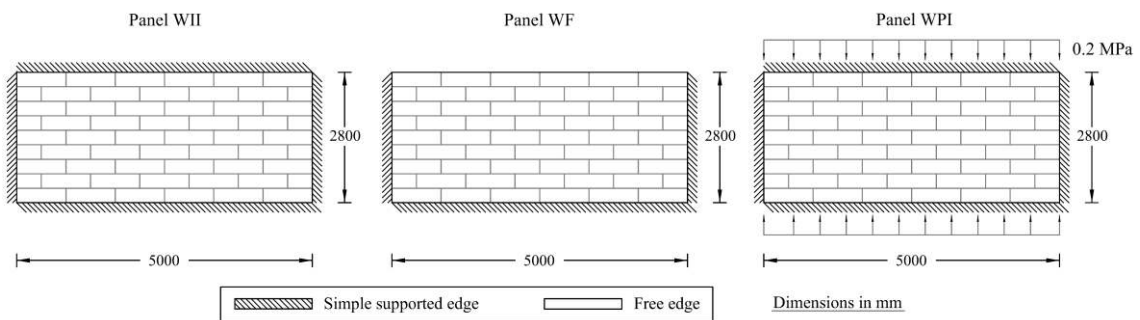
594

595 **Fig. 4.** Calibrated bending moment and torsional moment homogenized curves for the
 596 study of the panels tested by Chong et al. (1994).



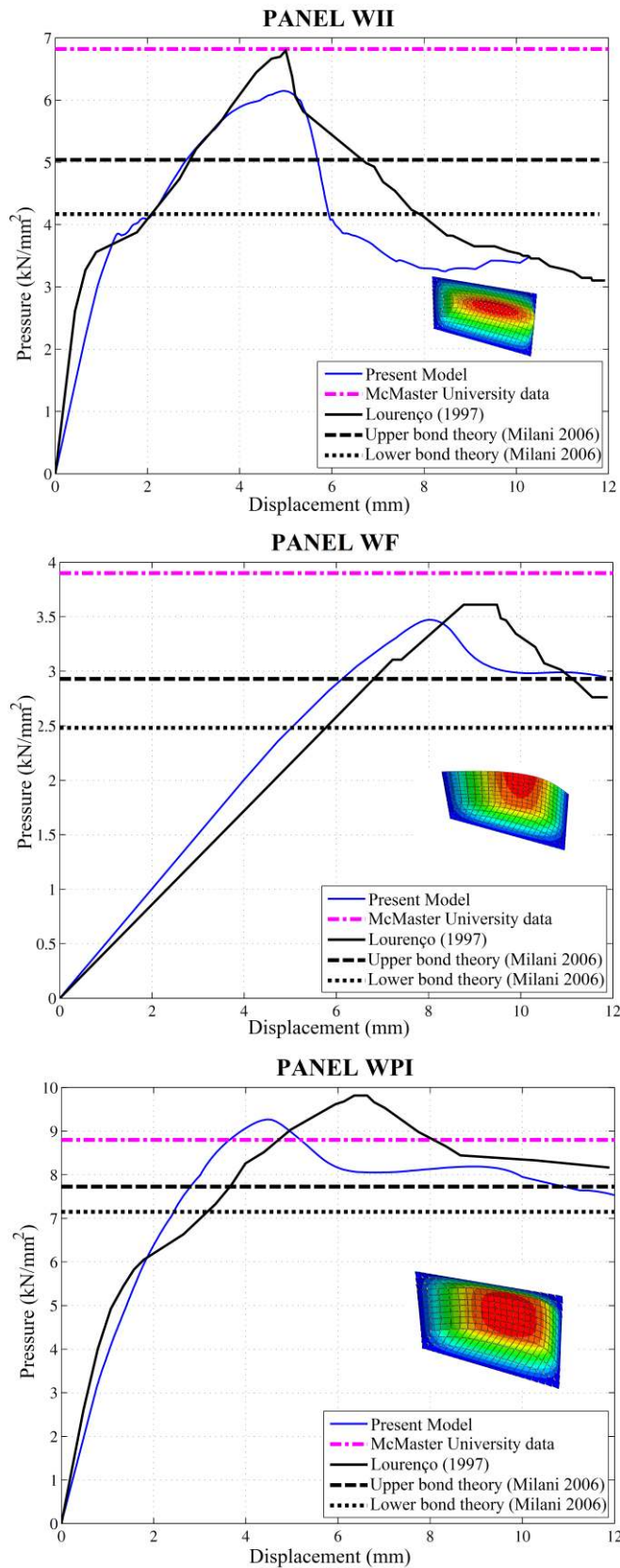
597

598 **Fig. 5.** The calibrated stress-strain curves obtained for the panels tested experimentally
 599 by Chong et al. (1994) at the University of Plymouth; input curves for each truss beam of
 600 the discrete system.



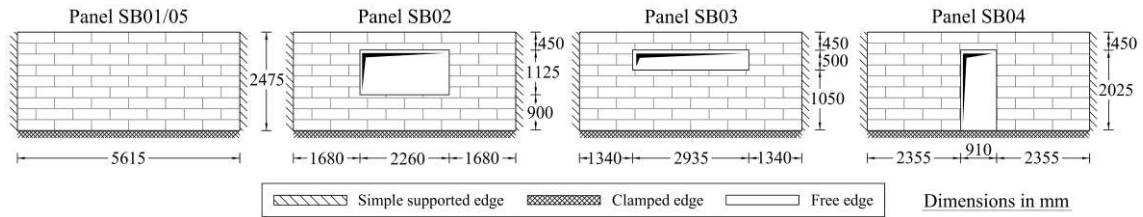
601

602 **Fig. 6.** Masonry panels out-of-plane loaded at University of McMaster (Gazzola and
 603 Drysdale 1986); description of the geometry and boundary conditions.



604

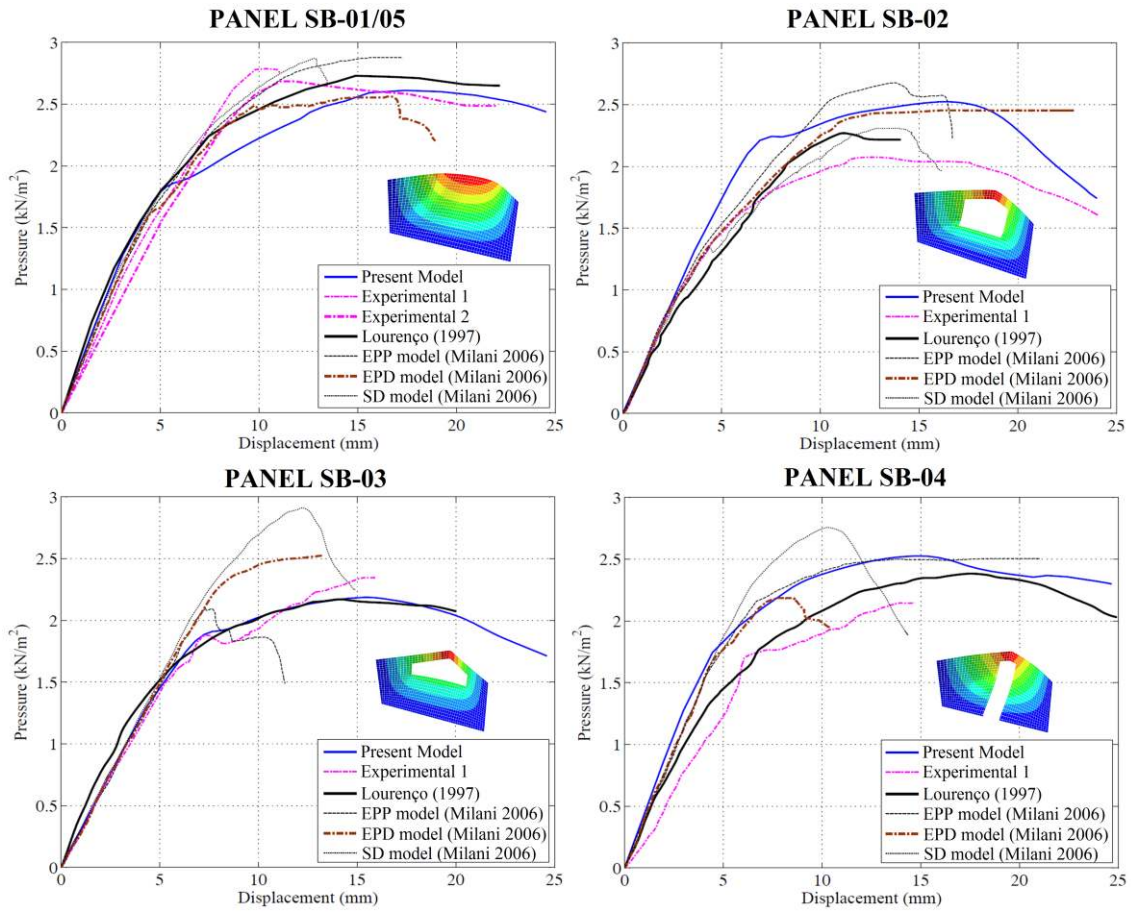
605 **Fig. 7.** Numerical and experimental curves of the panels experimentally tested by Gazzola
 606 and Drysdale (1986): pressure load vs displacement.



607

608 **Fig. 8.** Masonry panels out-of-plane loaded at University of Plymouth (Chong et al.

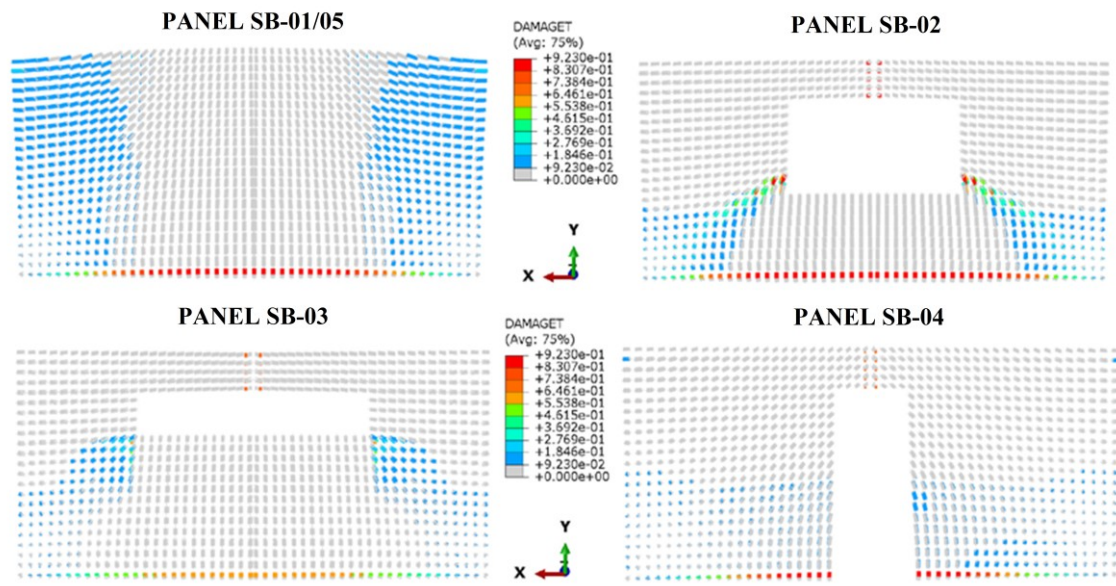
609 1994); description of the geometry and boundary conditions.



610

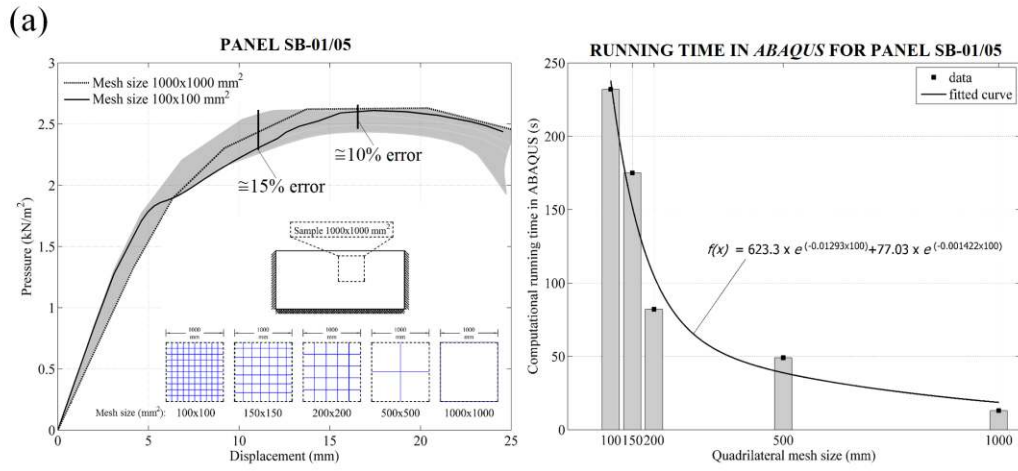
611 **Fig. 9.** Numerical and experimental curves of the panels experimentally tested by Chong

612 et al. (1994): pressure load vs displacement and deformed shapes at ultimate load level.

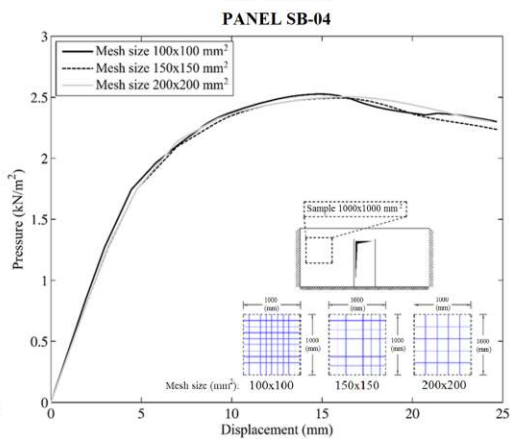
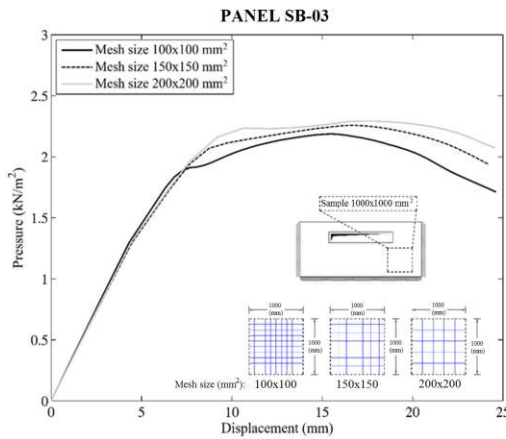
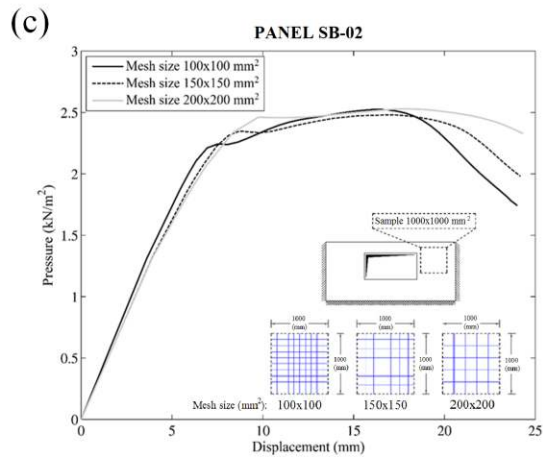
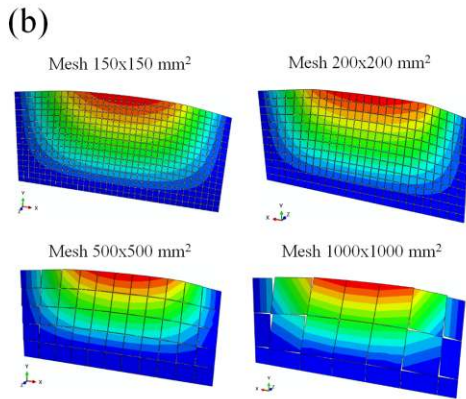
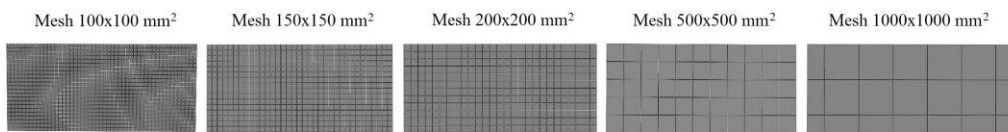


613

614 **Fig. 10.** Damage patterns obtained from the numerical analyses (ultimate load).



Panel SB01/05:



615

616 **Fig. 11.** (a) Mesh dependence for the SB-01/05 panel; (b) deformed shapes for the less

617 refined meshes for Panel SB-01/05; (c) mesh dependence study for the SB-02, SB-03 and

618 SB-04 panels.

619 **Table 1.** Mechanical properties adopted for the homogenization step for both McMaster
 620 and Plymouth University panels.

Parameter	Panels	
	McMaster	Plymouth
Young's Modulus of the mortar (MPa)	4000	3500
Young's Modulus of the brick (MPa)	15000	10000
Poisson coefficient (-)	0.20	0.20
Shear Modulus (MPa)	2000	1500
Cohesion, c (MPa)	$1.6 \times f_t$	$1.2 \times f_t$
Tensile strength f_t (MPa)	0.35	0.52
Compressive strength f_c (MPa)	20.0	2.0
Friction angle (ϕ) (degrees)	30.0	30.0
Linearized compressive cap angle (ψ) (degrees)	45.0	50.0
Mode I fracture energy, G_f^I (N/mm)	0.018	0.010
Mode II fracture energy, G_f^{II} (N/mm)	0.022	0.012
Elastic Parameters (for a mesh size: $H = 100$ mm; $e=10$ mm)		
K_n - axial truss (MPa)	236.74	157.83
K_n - torque truss (MPa)	191761	27874
Axial truss area (mm ²)	3750	2562.5
Torque truss area (mm ²)	500	500

621